EIAV–LacZ control ($n = 7$). Each mouse was injected with a total dosage of 90 µl of viral solution. Six sites per hindlimb muscle were injected with 5 µl per site.

Behavioural analysis

We analysed a rotarod task of the SOD1 mice by an Economex Rotarod instrument (Colombus Instruments) every ten days during the light phase of the 12 h light/12 h dark cycle. We performed three trials, and recorded the longest duration on the rod for every mouse. The timer is stopped when the mice fall from the rod or after an arbitrary limit of 180 s. Footprint analysis was also performed. Mouse hind paws were covered with ink to record walking patterns during continuous locomotion, and stride length was measured.

Histology and immunohistochemistry

Animals were perfused transcardially with 0.9% NaCl solution followed by ice-cold 4% paraformaldehyde. Spinal cord, brain and muscle tissues were dissected out and post-fixed overnight in the same solution and then transferred to 30% sucrose. Tissues were analysed by immunohistochemistry and X-gal (5-bromo-4-chloro-3-indolyl-β-D-galactoside) reaction. Spinal cord and brain were cut on a sliding cryostat microtome (Leica) at a thickness of 20 µm and collected as free-floating sections in PBS containing sodium azide. Primary antibodies were used as follows: rabbit anti-β-gal (1:1,000, Europe BioProducts); rabbit anti-CGRP (1:3,000, Sigma); mouse anti-ChAT (1:1,000, gift from B. K. Hartman and C. Cozari); CD3-T cells (1:50, Dako); P7/7-MHCII (1:100, Dako); goat anti-Glut-1 (1:20, Santa Cruz Biotechnology); and rabbit anti-albumin (1:250, ICN/Cappel).

VEGF ELISA

Dog osteosarcoma D17 cells were transduced in the presence of 8 mg ml^{-1} polybrene as described previously[24]. Cells were transduced with either EIAV–VEGF or EIAV–LacZ vectors. Transduced cells were passaged three times before analysis of transgene expression. One week post-transduction supernatants were collected and the VEGF levels measured by enzyme-linked immunosorbent assay (ELISA) (R&D Systems). The protein amino-acid sequences of dog VEGF are highly homologous to the human VEGF protein used in this kit, which has been used previously to determine dog VEGF levels[27]. To determine plasma VEGF levels, we collected blood in 10-ml vacuum tubes containing 100 µl of a 4% tri-sodium citrate solution, quickly centrifuged it and stored plasma fractions at −80 °C until analysis. VEGF ELISA assay measurements were also carried out using tissue samples from spinal cord and brain stem.

1. Mulder, D. W. Clinical limits of amyotrophic lateral sclerosis. *Adv. Neurol.* **36,** 15–22 (1982).
2. Carmeliet, P. Blood vessels and nerves: common signals, pathways and diseases. *Nature Rev. Genet.* **4,** 710–720 (2003).
3. Schratzberger, P. *et al.* Favorable effect of VEGF gene transfer on ischemic peripheral neuropathy. *Nature Med.* **6,** 405–413 (2000).
4. Jin, K. L., Mao, X. O. & Greenberg, D. A. Vascular endothelial growth factor: direct neuroprotective effect in *in vitro* ischemia. *Proc. Natl Acad. Sci. USA* **97,** 10242–10247 (2000).
5. Oosthuyse, B. *et al.* Deletion of the hypoxia-response element in the vascular endothelial growth factor promoter causes motor neuron degeneration. *Nature Genet.* **28,** 131–138 (2001).
6. Lambrechts, D. *et al.* VEGF is a modifier of amyotrophic lateral sclerosis in mice and humans and protects motoneurons against ischemic death. *Nature Genet.* **34,** 383–394 (2003).
7. Gurney, M. E. *et al.* Motor neuron degeneration in mice that express a human Cu,Zn superoxide dismutase mutation. *Science* **264,** 1772–1775 (1994).
8. Bruijn, L. I. *et al.* ALS-linked SOD1 mutant G85R mediates damage to astrocytes and promotes rapidly progressive disease with SOD1-containing inclusions. *Neuron* **18,** 327–338 (1997).
9. Azzouz, M. *et al.* Increased motoneuron survival and improved neuromuscular function in transgenic ALS mice after intraspinal injection of an adeno-associated virus encoding Bcl-2. *Hum. Mol. Genet.* **9,** 803–811 (2000).
10. Cleveland, D. W. & Rothstein, J. D. From Charcot to Lou Gehrig: deciphering selective motor neuron death in ALS. *Nature Rev. Neurosci.* **2,** 806–819 (2001).
11. Mazarakis, N. D. *et al.* Rabies virus glycoprotein pseudotyping of lentiviral vectors enables retrograde axonal transport and access to the nervous system after peripheral delivery. *Hum. Mol. Genet.* **10,** 2109–2121 (2001).
12. Wong, L. F. *et al.* Transduction patterns of pseudotyped lentiviral vectors in the nervous system. *Mol. Ther.* **9,** 101–111 (2004).
13. Rosen, D. R. Mutations in Cu/Zn superoxide dismutase gene are associated with familial amyotrophic lateral sclerosis. *Nature* **364,** 362 (1993).
14. Ferreirinha, F. *et al.* Axonal degeneration in paraplegin-deficient mice is associated with abnormal mitochondria and impairment of axonal transport. *J. Clin. Invest.* **113,** 231–242 (2004).
15. Sagot, Y., Rosse, T., Vejsada, R., Perrelet, D. & Kato, A. C. Differential effects of neurotrophic factors on motoneuron retrograde labeling in a murine model of motoneuron disease. *J. Neurosci.* **18,** 1132–1141 (1998).
16. Dal Canto, M. C. & Gurney, M. E. Neuropathological changes in two lines of mice carrying a transgene for mutant human Cu,Zn SOD, and in mice overexpressing wild type human SOD: a model of familial amyotrophic lateral sclerosis (FALS). *Brain Res.* **676,** 25–40 (1995).
17. Wang, L. J. *et al.* Neuroprotective effects of glial cell line-derived neurotrophic factor mediated by an adeno-associated virus vector in a transgenic animal model of amyotrophic lateral sclerosis. *J. Neurosci.* **22,** 6920–6928 (2002).
18. Kaspar, B., Llado, J., Sherkat, N., Rothstein, J. & Gage, F. Retrograde viral delivery of IGF-1 prolongs survival in a mouse ALS model. *Science* **301,** 839–842 (2003).
19. Fukuda, R. *et al.* Insulin-like growth factor 1 induces hypoxia-inducible factor 1-mediated vascular endothelial growth factor expression, which is dependent on MAP kinase and phosphatidylinositol 3-kinase signaling in colon cancer cells. *J. Biol. Chem.* **277,** 38205–38211 (2002).
20. Hellstrom, A. *et al.* Low IGF-I suppresses VEGF-survival signaling in retinal endothelial cells: direct correlation with clinical retinopathy of prematurity. *Proc. Natl Acad. Sci. USA* **98,** 5804–5808 (2001).
21. Mitchell, J. D., Wokke, J. H. & Borasio, G. D. Recombinant human insulin-like growth factor I (rhIGF-I) for amyotrophic lateral sclerosis/motor neuron disease. *Cochrane Database Syst. Rev.* **3,** CD002064 (2002).
22. Azzouz, M. *et al.* Multicistronic lentiviral vector-mediated striatal gene transfer of aromatic L-amino acid decarboxylase, tyrosine hydroxylase, and GTP cyclohydrolase I induces sustained transgene expression, dopamine production, and functional improvement in a rat model of Parkinson's disease. *J. Neurosci.* **22,** 10302–10312 (2002).
23. Bienemann, A. S. *et al.* Long-term replacement of a mutated nonfunctional CNS gene: reversal of hypothalamic diabetes insipidus using an EIAV-based lentiviral vector expressing arginine vasopressin. *Mol. Ther.* **7,** 588–596 (2003).
24. Mitrophanous, K. *et al.* Stable gene transfer to the nervous system using a non-primate lentiviral vector. *Gene Ther.* **6,** 1808–1818 (1999).
25. Rohll, J. B. *et al.* Design, production, safety, evaluation, and clinical applications of nonprimate lentiviral vectors. *Methods Enzymol.* **346,** 466–500 (2002).
26. Martin-Rendon, E., White, L. J., Olsen, A., Mitrophanous, K. A. & Mazarakis, N. D. New methods to titrate EIAV-based lentiviral vectors. *Mol. Ther.* **5,** 566–570 (2002).
27. Mohammed, S. I. *et al.* Effects of the cyclooxygenase inhibitor, piroxicam, on tumor response, apoptosis, and angiogenesis in a canine model of human invasive urinary bladder cancer. *Cancer Res.* **62,** 356–358 (2002).

··

Premature ageing in mice expressing defective mitochondrial DNA polymerase

Aleksandra Trifunovic[1,2], **Anna Wredenberg**[1,2], **Maria Falkenberg**[1], **Johannes N. Spelbrink**[3], **Anja T. Rovio**[3], **Carl E. Bruder**[4], **Mohammad Bohlooly-Y**[4], **Sebastian Gidlöf**[1,2], **Anders Oldfors**[5], **Rolf Wibom**[6], **Jan Törnell**[4], **Howard T. Jacobs**[3] & **Nils-Göran Larsson**[1,2]

[1]*Department of Medical Nutrition and* [2]*Department of Biosciences, Karolinska Institutet, Novum, Karolinska University Hospital, S-141 86 Stockholm, Sweden*
[3]*Institute of Medical Technology and Tampere University Hospital, FIN-33014 University of Tampere, Finland*
[4]*Astra Zeneca R&D, S-431 83 Mölndal, Sweden*
[5]*Department of Pathology, Sahlgrenska University Hospital, S-413 45 Göteborg, Sweden*
[6]*Department of Laboratory Medicine, Karolinska Institutet, Karolinska University Hospital, S-141 86 Stockholm, Sweden*

Point mutations and deletions of mitochondrial DNA (mtDNA) accumulate in a variety of tissues during ageing in humans[1]**, monkeys**[2] **and rodents**[3]**. These mutations are unevenly distributed and can accumulate clonally in certain cells, causing a mosaic pattern of respiratory chain deficiency in tissues such as heart**[4]**, skeletal muscle**[5] **and brain**[6]**. In terms of the ageing process, their possible causative effects have been intensely debated because of their low abundance and purely correlative connection with ageing**[7,8]**. We have now addressed this question experimentally by creating homozygous knock-in mice that express a proof-reading-deficient version of PolgA, the nucleus-encoded catalytic subunit of mtDNA polymerase. Here we show that the knock-in mice develop an mtDNA mutator phenotype with a threefold to fivefold increase in the levels of point mutations, as well as increased amounts of deleted mtDNA. This increase in somatic mtDNA mutations is associated with reduced lifespan and premature onset of ageing-related phenotypes such as weight loss, reduced subcutaneous fat, alopecia (hair loss), kyphosis**

(curvature of the spine), osteoporosis, anaemia, reduced fertility and heart enlargement. Our results thus provide a causative link between mtDNA mutations and ageing phenotypes in mammals.

The mtDNA polymerases of yeast and animal cells have an inherent $3'-5'$ exonuclease activity necessary for proof-reading newly synthesized mtDNA[9–11]. The exonuclease activity of the *Saccharomyces cerevisiae* mtDNA polymerase, Mip1p, is critically dependent on specific, conserved aspartate residues located in three 'exonuclease' domains[10,11]. We created knock-in mice (Fig. 1a–d) expressing mtDNA polymerase with an altered catalytic PolgA subunit that contained an alanine instead of the critical aspartate residue of the second exonuclease domain (D257A). We first generated the *PolgA^mutNeo* allele (Fig. 1a) in embryonic stem cells (Fig. 1b) and obtained germline transmission of this allele (Fig. 1c, d). Next, we excised the *Frt*-site-flanked neomycin-resistance gene by mating heterozygous *PolgA^mutNeo* mice with a line ubiquitously expressing *Flp*-recombinase[12], thus generating heterozygous *PolgA^mut* (+/*PolgA^mut*) mice (Fig. 1a, c, d). We chose to perform this *in vivo* excision procedure because others have shown that the presence of the neomycin resistance gene in a targeted locus can result in a hypomorphic allele[13]. Finally, we performed intercrosses of +/*PolgA^mut* mice to generate homozygous knock-in mice (*PolgA^mut*/*PolgA^mut*), hereafter denoted 'mtDNA-mutator' mice.

We analysed recombinant mtDNA polymerase holoenzyme complexes *in vitro* and found that mtDNA polymerase containing a PolgA subunit bearing the Asp → Ala exonuclease domain mutation had a profound reduction of exonuclease activity (Fig. 1e). Others have shown that certain exonuclease-deficient versions of yeast mtDNA polymerase have reduced capacity to synthesize DNA[10,11]. However, no decrease in DNA polymerase activity was observed in biochemical assays with recombinant exonuclease-deficient mtDNA polymerase (Fig. 1f) or in mitochondrial extracts from heterozygous knock-in (+/*PolgA^mut*) or mtDNA-mutator mice (Fig. 1g).

The mtDNA-mutator mice had a normal appearance until the age of ~25 weeks, when we first noted slight kyphosis and alopecia. As the animals got older the kyphosis became marked and varying degrees of alopecia appeared (Fig. 2a). The median lifespan of the mtDNA-mutator mice was ~48 weeks and all of them died before the age of 61 weeks (Fig. 2e). Weight gain of the mtDNA-mutator mice started to decelerate from ~15–20 weeks of age and weight loss was noted from ~24 weeks of age (Fig. 2f, g). Alopecia is common in human ageing[14]. In addition, a decrease in body weight occurs in humans older than 60 years[15] and is also well documented in mice older than ~1.5 years[16].

We performed quantitative assessments of body composition with X-ray densitometry of the whole mouse (Fig. 2c) or dissected
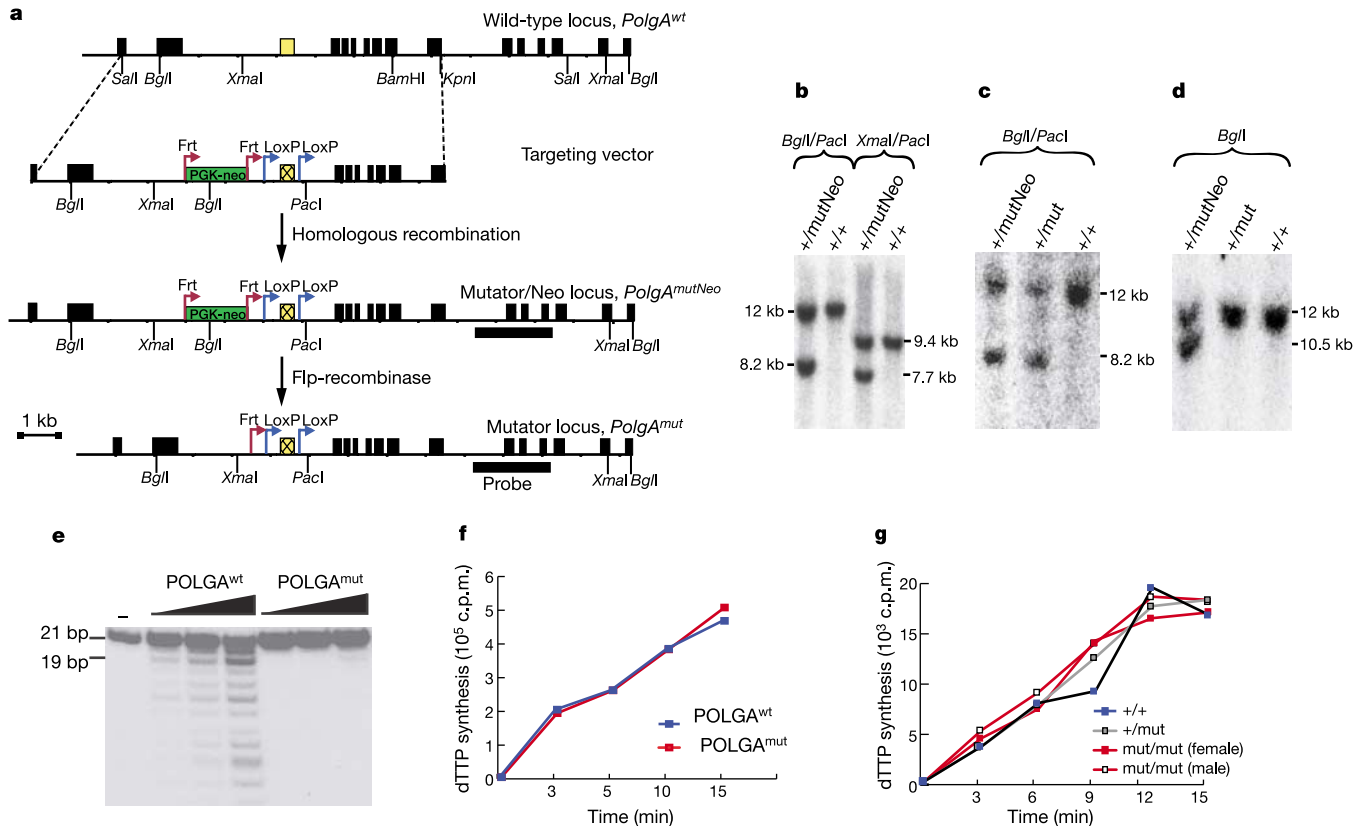

Figure 1 Creation of mtDNA-mutator mice and biochemical assays of DNA polymerase and exonuclease activities. **a**, Restriction map of the 5′ region of the wild-type *PolgA* locus (*PolgA^wt*), the targeting vector, the *PolgA* locus after homologous recombination (*PolgA^mutNeo*) and the mutator locus obtained after *Flp*-recombinase-mediated excision of the *PGK-neo* gene (*PolgA^mut*). The sequence of exon 3 (yellow box) of the targeting vector was changed to encode an alanine instead of the highly conserved aspartate residue. The thick black line indicates the probe used to screen for homologous recombination. **b**, Digestion of ES cell DNA with the restriction endonucleases *Bgl*I/*Pac*I or *Xma*I/*Pac*I generates a novel fragment of ~8.2 kb and ~7.7 kb, respectively, in clones that are heterozygous for *PolgA^mutNeo*. **c, d**, Mice heterozygous for *PolgA^mutNeo* (+/mutNeo) were

mated to *Flp*-mice to excise the *Frt*-flanked *PGK-neo* cassette to obtain heterozygous *PolgA^mut* mice (+/mut). **e**, Biochemical assays of exonuclease activity. Recombinant human POLGA proteins were co-expressed with the human accessory subunit, POLGB, to obtain recombinant mtDNA polymerase holoenzyme. The enzyme containing the POLGA^wt polypeptide exhibits exonuclease activity, whereas the POLGA^mut-containing enzyme lacks this activity. **f**, DNA synthesis activities with recombinant holoenzymes consisting of human POLGA^wt or POLGA^mut and POLGB. **g**, DNA-synthesis activities in mitochondrial extracts isolated from liver of wild-type (+/+), heterozygous *PolgA^mut* mice (+/mut) and mtDNA-mutator mice (*PolgA^mut*/*PolgA^mut*; mut/mut).

femur bones (Fig. 2d). The ratio of lean body mass to length was normal, whereas the fat content was reduced in mtDNA-mutator mice (Fig. 2c), consistent with their overall appearance (Fig. 2a) and histological analyses of subcutaneous fat (Fig. 2b). In humans, body fat decreases with age after 65 years and a reduction in subcutaneous fat is common in the ageing skin[14]. Measurements of whole-body bone mineral density (BMD) showed a clear reduction at the age of 40 weeks in mtDNA-mutator mice (Fig. 2c), consistent with the clinical features of osteoporosis (marked kyphosis; Fig. 2a). There was a tendency to reduction in the ratio of whole-body bone mineral content (BMC) to length at 40 weeks of age (Fig. 2c). We

also analysed dissected femur, to improve the precision of the BMD and BMC measurements, and found no difference between mtDNA-mutator and wild-type mice at 20 weeks of age. However, there was a clear reduction in BMD (Fig. 2d), BMC (not shown) and BMC/length (Fig. 2d) in femur of mtDNA-mutator mice at the age of 40 weeks. In conclusion, the X-ray densitometry revealed a change in body composition, with reduced fat content and development of osteoporosis in the mtDNA-mutator mice. Human ageing is similarly accompanied by kyphosis and osteoporosis[14]. Osteoporosis is also found in ageing rodents as demonstrated by decreased bone densities in aged wild-type mice[17].
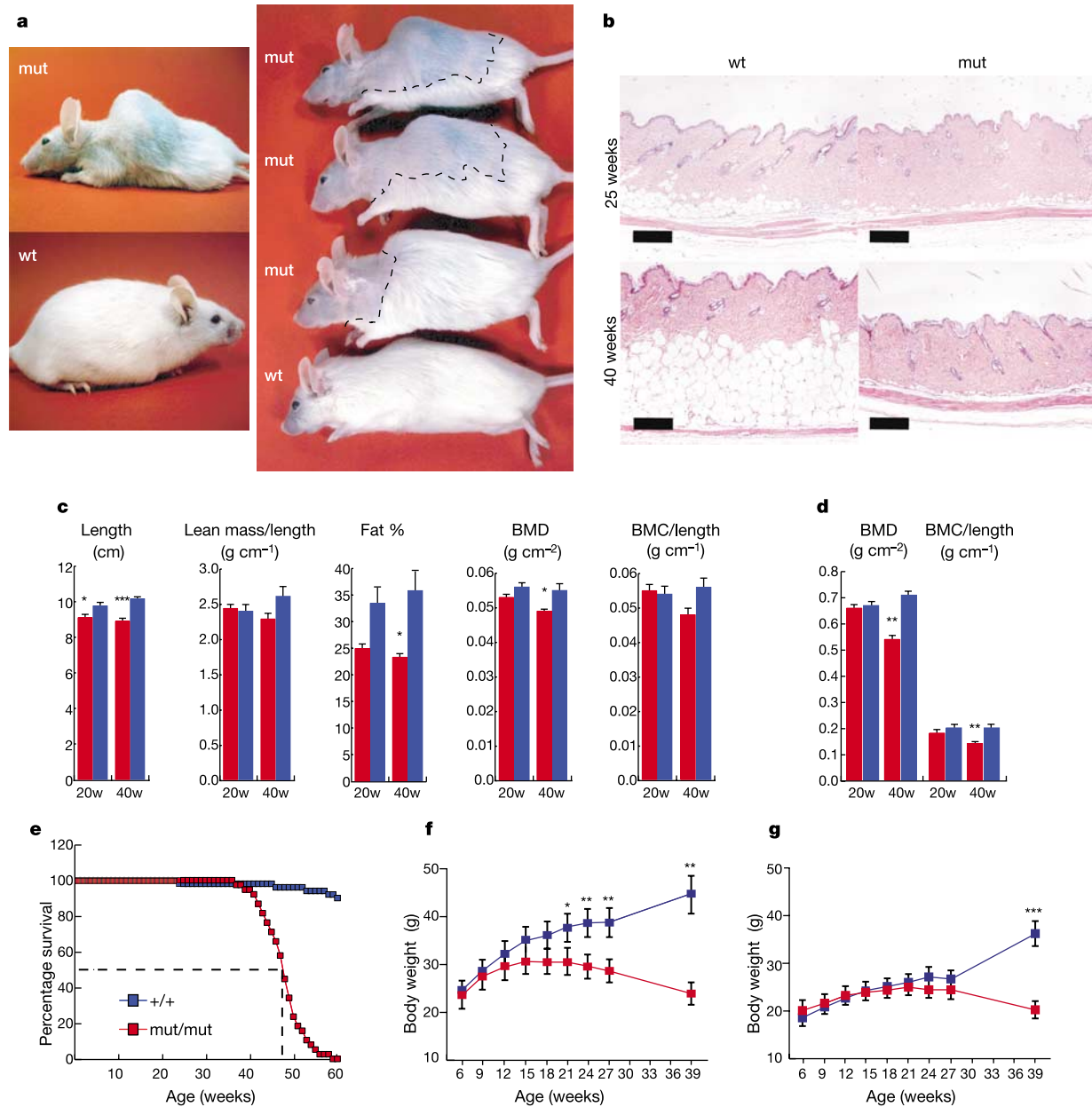

Figure 2 Ageing-related phenotypes observed in mtDNA-mutator mice. **a**, The mtDNA-mutator mice show reduced body size, kyphosis, reduced hair density and different stages of alopecia (delineated by dashed line) in comparison with littermate wild-type (wt) mice at the age of ~40–45 weeks. **b**, Haematoxylin- and eosin-stained cross-section of dorsal skin from 25- and 40-week-old wild-type (wt; $n = 3$ animals at each time point) and mtDNA-mutator (mut; $n = 3$) mice. Scale bar, 100 μm. **c**, Quantitative assessment of body length, lean mass, fat content, BMD and BMC by X-ray densitometry of mtDNA-mutator mice (red bars) and wild-type littermates (blue bars). **d**, Quantitative

assessment of BMD and BMC by X-ray densitometry of dissected femur from mtDNA-mutator mice (red bars) and wild-type littermates (blue bars). 20w, 20 weeks; 40w, 40 weeks. **e**, Survival curves for wild-type ($n = 50$; blue line) and mtDNA-mutator ($n = 38$; red line) mice. **f**, Body weight curves for male wild-type ($n = 5$–13 mice at the different time points; blue line) and mtDNA-mutator ($n = 8$–10; red line) mice. **g**, Body weight curves for female wild-type ($n = 5$–7; blue line) and mtDNA-mutator ($n = 9$–11; red line) mice. Asterisk, $P < 0.05$; double asterisk, $P < 0.01$; triple asterisk, $P < 0.001$, Student's t-test. All error bars indicate s.e.m.

We found significantly lower haemoglobin concentrations in peripheral blood ($P < 0.001$, Student's t-test) of mtDNA-mutator mice (81 ± 3 g per litre, mean $\pm$ s.e.m; $n = 9$ analysed animals) in comparison with wild-type littermates (106 ± 3 g per litre; $n = 8$) at the age of 25 weeks. The anaemia in mtDNA-mutator mice was macrocytic and hypochromic (Supplementary Table 1). In addition, we observed extramedullary haematopoiesis in the liver (Fig. 3b) and spleen enlargement (Supplementary Tables 2 and 3), with increased relative contribution of red pulp (Fig. 3a) in mtDNA-mutator mice. Increased haematopoiesis in the spleen and foci of haematopoiesis in the liver are common findings in ageing mice[16]. It should also be noted that anaemia of unknown aetiology is a frequent clinical problem in elderly humans[18].

The heart weight in relation to body weight was increased in mtDNA-mutator mice (Supplementary Table 3). The 40-week-old mtDNA-mutator mice also had an enlarged lumen of the left ventricle of the heart (Fig. 3c). Increases of heart weight and left ventricle hypertrophy are normally found in the ageing human heart[14,19]. Cardiomyopathy is common with increasing age in wild-type mice[16]. We performed enzyme histochemical staining of heart muscle tissue sections from mtDNA-mutator mice and found a mosaic pattern, with cytochrome c oxidase deficiency in some cardiomyocytes (Fig. 3d), similar to findings in ageing human hearts[4]. In accordance with this finding, light microscopy of thin sections of heart muscle showed that some cardiomyocytes had a vacuolated appearance because of accumulations of enlarged mitochondria (Fig. 3e). Electron microscopy studies of tissue sections from heart confirmed that there was an accumulation of abnormal mitochondria in a subset of the cardiomyocytes (Fig. 3f) in mtDNA-mutator mice.

A profound reduction in fertility of mtDNA-mutator mice of both sexes was found. In matings between 15 mtDNA-mutator females and 15 wild-type males, 14 of the females did become pregnant, each giving birth to one or two litters of normal size. However, the females did not become pregnant again after the age of 20 weeks, despite being continuously exposed to males for several months. We also set up matings over several months between 8 mtDNA-mutator males and 16 wild-type females, but obtained only a single, small litter. Testes of the mtDNA-mutator males were considerably smaller than wild-type testes from 12 weeks of age onwards (Fig. 3g; Supplementary Tables 2 and 3). Inspection of testes from mtDNA-mutator mice revealed reduced sperm content
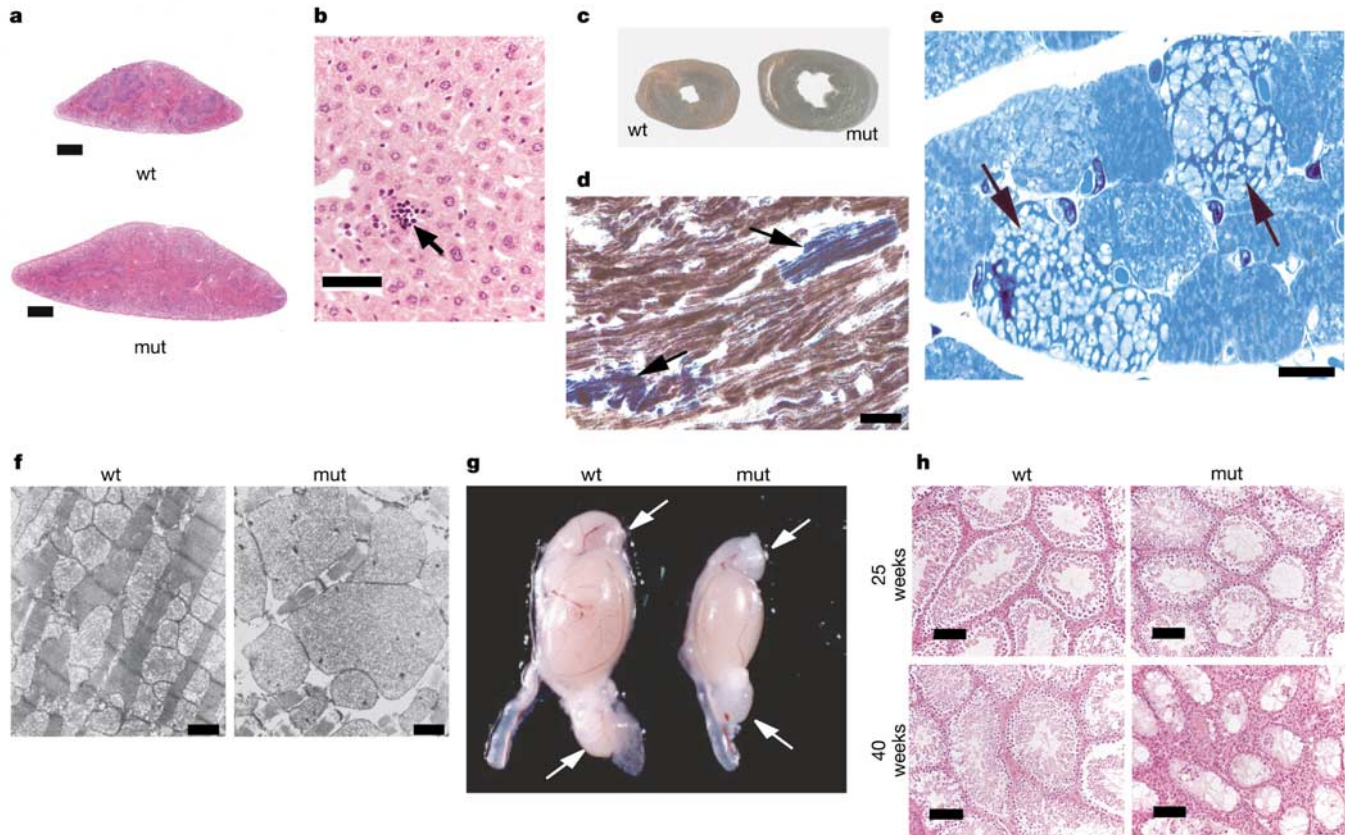

Figure 3 Histological analyses of different tissues from mtDNA-mutator mice.
a, Haematoxylin- and eosin-stained sections of spleen of wild-type (wt; $n = 8$ analysed animals) and mtDNA-mutator mice (mut; $n = 8$) at age 25 weeks. Scale bar, 0.5 mm.
b, Haematoxylin- and eosin-stained section from the liver of mtDNA-mutator ($n = 8$) and wild-type ($n = 8$, not shown) mice at age 25 weeks. Extramedullary haematopoiesis (arrow) is present in mtDNA mutator mice. Scale bar, 50 μm. **c**, Unstained thick sections of heart from wild-type ($n = 3$) and mtDNA-mutator mice ($n = 3$) at age 40 weeks.
d, Enzyme histochemical double staining for cytochrome c oxidase (COX) and succinate dehydrogenase (SDH) activities in heart of an mtDNA-mutator mouse at age 40 weeks. The presence of both COX and SDH activity results in a brown colour. A mosaic pattern is present in the mtDNA-mutator mouse heart and some cardiomyocytes appear blue (arrows) because of a lack of COX activity (catalytic subunits are mtDNA encoded) and preserved SDH activity (all subunits are nucleus encoded). Scale bar, 20 μm. A total of three mtDNA-mutator and three wild-type mice were analysed. **e**, Light microscopic image of a thin section of Epon-embedded heart muscle from an mtDNA-mutator mouse at age 40 weeks shows cardiomyocytes with accumulation of enlarged mitochondria (arrows). Scale bar, 10 μm. **f**, Electron micrographs of cardiomyocytes from wild-type ($n = 3$) and an mtDNA-mutator ($n = 3$) mice. Some cardiomyocytes of the mtDNA-mutator mouse contains enlarged abnormally shaped mitochondria. Scale bar, 1 μm.
g, Testis from wild-type ($n = 13$) and mtDNA-mutator ($n = 13$) mice at the age of 25 weeks. The size of the testis is reduced and no sperm is visible on macroscopic inspection of the epididymis (arrows) of the mtDNA-mutator mouse. **h**, Cross-sections of testis of wild-type ($n = 4–6$) and mtDNA-mutator ($n = 4–6$) mice at 25 and 40 weeks of age. Scale bar, 100 μm.
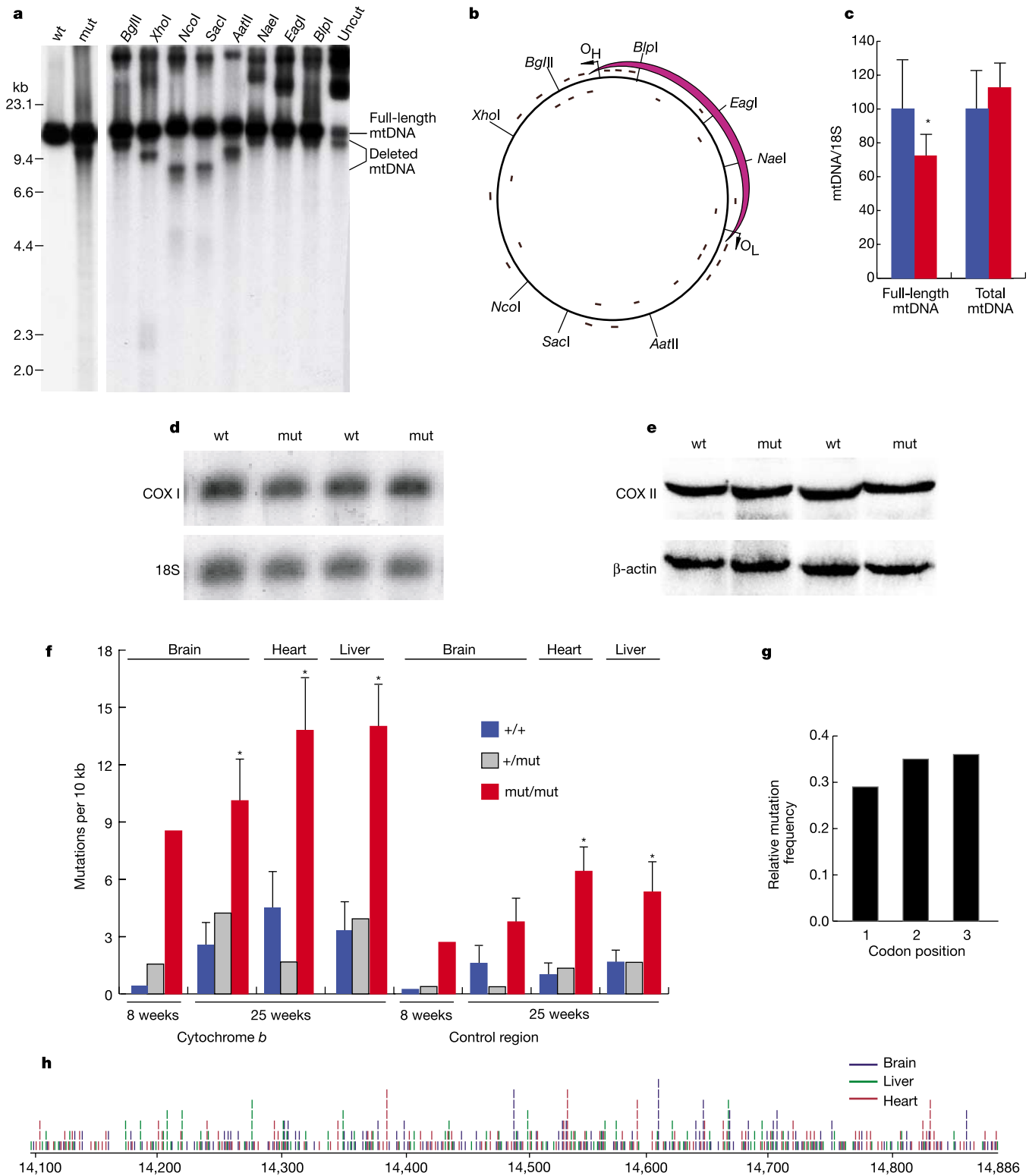
Figure 4 Analysis of mtDNA. **a**, Southern blot analysis of *Bgl*II-digested liver mtDNA from a wild-type and an mtDNA-mutator mouse at age 25 weeks (lane 1–2). Southern blot analysis of restriction-enzyme-digested mtDNA from an mtDNA-mutator mouse at age 25 weeks (lanes 3–11). **b**, The deleted mtDNA region is indicated with a purple arc. The black bars represent 29 strand-specific oligonucleotide probes used to map the mtDNA deletions. Oligonucleotides identical to the L-strand of mtDNA are inside and those identical to the H-strand are outside the circle. **c**, Quantification of mtDNA levels (mean ± s.e.m; asterisk, $P < 0.01$, Student's *t*-test) in liver from mtDNA-mutator (red bars; $n = 6$) and wild-type (blue bars; $n = 6$) mice at age 12–40 weeks. **d**, Northern blot analysis of cytochrome *c* oxidase subunit I (COX I) transcript levels in heart of wild-type and mtDNA-mutator mice at age 40 weeks. **e**, Western blot analysis of cytochrome *c* oxidase subunit II polypeptide (COX II) levels in heart of wild-type and mtDNA-mutator mice at age 25 weeks. **f**, mtDNA mutation loads in mtDNA-mutator (mut/mut; red bars), heterozygous *PolgA* ^{mut} (+/mut; grey bars) and wild-type (+/+; blue bars) mice. The bars indicate mean values. The standard deviation (indicated by error bars) was calculated in groups where DNA from three or four mice of the same genotype was sequenced. Absence of error bars indicates cases where only one or two animals were analysed. Asterisk, $P < 0.005$, Student's *t*-test. **g**, Relative mutation frequencies at all codon positions in the cytochrome *b* gene. **h**, Positions of individual mutations in the cytochrome *b* gene of brain (blue), heart (red) and liver (green) from 25-week-old mtDNA-mutator mice.

of the epididymis (Fig. 3g) and histological analyses of testis sections confirmed reduced sperm content in epididymis of mtDNA-mutator mice (data not shown). We observed severe testicular tubular degeneration with complete absence of sperm in 40-week-old mtDNA-mutator mice (Fig. 3h). In humans, female fertility decreases with age and males develop an age-associated decline in sperm count[20]. Degenerated tubules may occupy as much as 60% of the testis in aged, wild-type mice[21].

We performed Southern blot analyses and found a widespread tissue distribution of a class of shorter mtDNA molecules, up to ~12 kilobases (kb) in length, in mtDNA-mutator mice (Fig. 4a and Supplementary Fig. 1). Further analyses were performed with restriction enzymes that have single recognition sites in normal mouse mtDNA (Fig. 4a). The restriction enzymes *Nae*I, *Eag*I and *Blp*I did not digest the shorter mtDNA molecules, whereas the restriction enzymes *Bgl*II, *Xho*I, *Nco*I, *Sac*I and *Aat*II did digest the shorter molecules and gave a DNA fragment pattern showing that the shorter species behaved as a linear, subgenomic—that is, deleted—mtDNA molecule (Fig. 4a). The amount of deleted mtDNA did not change over time and the levels of deleted mtDNA were comparable in all investigated tissues (Supplementary Fig. 1). Southern blot analyses with radiolabelled oligonucleotides or short DNA fragments (Supplementary Fig. 1) localized the commonly deleted region to the small arc between O_H and O_L (Fig. 4b), which is consistent with the results from the restriction enzyme analysis (Fig. 4a). The mean level of full-length mtDNA was ~70% of the level in wild-type mice (Fig. 4c). The reduced copy number of full-length mtDNA did not affect overall mtDNA expression; the steady-state levels of the mtDNA-encoded cytochrome *c* oxidase subunit 1 messenger RNA (Fig. 4d) and the mtDNA-encoded cytochrome *c* oxidase subunit 2 polypeptide (Fig. 4e) were normal. These findings are consistent with our previous observation that ~35–40% general reduction of mtDNA copy number in heterozygous mitochondrial transcription factor A knockout ($+/Tfam^-$) mice has minimal effects on mtDNA expression and respiratory chain function[22].

We cloned and sequenced segments of mtDNA from brain, heart and liver, and found that mtDNA-mutator mice contain an increased load (~3–5 times) of somatic mtDNA point mutations (Fig. 4f). The mutation background from PCR (polymerase chain reaction) was subtracted when the mtDNA mutation load was calculated. We also discarded the few multiple occurrences of a single mutation because they could reflect clonal expansion, which includes selection and/or genetic drift in addition to *de novo* mutagenesis. The presented frequency of somatic mtDNA mutations (Fig. 4f) thus represents a conservative minimal estimate. We combined the cytochrome *b* gene sequencing results from all tissues and time points of mtDNA-mutator mice (>600 individual mutations) and found that all codon positions were equally affected (Fig. 4g). In addition, the mutations were evenly distributed along the cytochrome *b* gene (Fig. 4h). There were thus no obvious mutational hot spots in mtDNA-mutator mice, although mutation load in the non-coding control region was lower than in the cytochrome *b* gene. The mutation load in heterozygous mice (Fig. 4f) was indistinguishable from that of wild-type littermates, and these mice displayed no phenotype, showing that the $PolgA^{mut}$ mutation is recessive.

We further characterized respiratory chain function in the hearts of mtDNA-mutator mice (Supplementary Fig. 2) because of the findings of focal cytochrome *c* oxidase deficiency (Fig. 3d) and increased mitochondrial mass in some cardiomyocytes (Fig. 3e, f). We found slightly increased citrate synthase activities, consistent with a moderate increase in mitochondrial mass. There was a progressive reduction of respiratory chain enzyme activities and of mitochondrial ATP production rates (MAPR) in the hearts of mtDNA-mutator mice. The observed decline of respiratory chain enzyme activities and MAPR had profiles consistent with the

suggestion that the deficiencies were induced by mutations of mtDNA (Supplementary Fig. 2).

Our results establish a direct, experimental link between increased levels of somatic mtDNA mutations, respiratory chain dysfunction and phenotypes present in ageing mammals. The enhanced mtDNA mutation load of the mtDNA-mutator mouse is clearly generated somatically, because it is not shared with heterozygous or wild-type littermates. However, the detailed kinetics of accumulation of somatic mtDNA mutations remains to be elucidated. The mutation load is already substantial by 2 months, and is also rather uniform between tissues, suggesting that much of the mutation accumulation may occur during embryonic and/or fetal development. The onset of premature ageing is not accompanied, temporally, by a large *de novo* accumulation of mtDNA mutations around 6 months. Rather, it seems more plausible to ascribe it to cumulative physiological damage caused by the high mutation load during adult life, and/or to segregation or clonal expansion of specific mutations, as supported by the observed mosaicism for respiratory chain deficiency in the heart. Loss of vital cells in which mtDNA mutations have accumulated beyond a critical threshold (for example, through apoptosis or replicative senescence associated with telomere shortening brought on by oxidative stress) may be the critical process that manifests as premature ageing and reduced lifespan. We have previously generated a series of tissue-specific *Tfam* knockout mouse strains with reduced mtDNA expression and severe respiratory chain deficiency in different organs, accompanied by increased cell death and/or apoptosis[23–26]. However, we found only minor or no induction of defence mechanisms against reactive oxygen species (ROS) in these knockouts[24,27]. The possible involvement of increased ROS production as a mechanism of physiological damage leading to premature ageing in the mtDNA-mutator mouse should nevertheless not be discounted. Unlike tissue-specific *Tfam* knockouts, in which the effects on respiration and oxidative phosphorylation are essentially quantitative, the mtDNA-mutator creates an apparently random set of point mutations in genes for respiratory chain subunits. These may be expected to exhibit qualitative, as well as quantitative, abnormalities, of which increased ROS production and proton leak are likely consequences. The mtDNA-mutator mice will thus be a valuable tool for future experiments to determine whether the consequences of increased somatic mtDNA mutation can be counteracted by genetic, pharmacological or dietary interventions that affect ROS formation, bioenergetic homeostasis, cell death, apoptosis or other pathophysiological effects of respiratory chain dysfunction. Such approaches may allow us to design strategies to antagonize or delay deleterious consequences of naturally occurring somatic mtDNA mutations in human ageing. ☐

Methods

Creation of mtDNA-mutator mice

A genomic clone containing exons 1–16 of the mouse *PolgA* gene was isolated from a 129/SvJ λ Fix II phage library (Stratagene). A *Sal*I–*Kpn*I *PolgA* fragment of 8.1 kb (Fig. 1a) was cloned into pBluescript II SK+ (pBS, Stratagene) to generate plasmid pST1. A *Bam*HI–*Sal*I fragment of 3.6 kb (Fig. 1a) was cloned into pBS to generate plasmid pST4. The inserts of plasmids pST1 and pST4 were completely sequenced. The plasmid pST8 was constructed by cloning a 1.4-kb *Sac*I fragment of pST1 containing exon 3 (which encodes exonuclease domain 2) into pBS and used for site-directed mutagenesis with the oligonucleotides E3-1 (5′-gttagtggtggggcacaatgtttccttt gcccgagccc-3′) and E3-2 (5′-gggctcgggcaaaggaaacattgtgccccaccactaac-3′) to change the aspartic acid codon (GAC) at position 257 to an alanine codon (GCC). The pDelboy plasmid (provided by D. Rossi) contains an *Frt*-site-flanked neomycin gene expressed from the phosphoglycerate kinase promoter (*PGK-neo*), two *loxP* sites and a cassette containing the herpes simplex virus thymidine kinase gene expressed from the phosphoglycerate kinase promoter (*PGK-HSV-TK*). The plasmid pST7 was constructed by exchanging one *loxP* site and the *PGK-HSV-TK* cassette in pDelboy with a DNA fragment containing a *Sac*I–*loxP*–*Pac*I sequence. The insert of pST8 was introduced into the *Sac*I-site of pST7 to generate pST9. Plasmid pST6 was generated by replacing the 1.4-kb *Sac*I fragment of pST1 with a DNA fragment containing a *Kpn*I/*Eco*RI/*Pac*I polylinker sequence. The final targeting vector for introducing the $PolgA^{mutNeo}$ allele was obtained by ligating a 3.6-kb *Xho*I/*Pac*I fragment from pST9 into pST6. The composition of DNA constructs was confirmed by restriction-

enzyme mapping and partial sequencing after each cloning step. The targeting vector was linearized with *Sal*I and electroporated into 129 R1 embryonic stem (ES) cells. A total of 61 ES cell clones were subjected to Southern blot analysis and nine specifically targeted clones were found (Fig. 1b). We generated chimaeras by blastocyst injection of ES cells and obtained germline transmission of the *PolgA^{mutNeo}* allele from two clones. Mice heterozygous for the *PolgA^{mutNeo}* allele were mated with transgenic C57BL/6 mice ubiquitously expressing *Flp*-recombinase[12] to remove the *PGK-Neo* gene, thus generating heterozygous *PolgA^{mut}* mice (Fig. 1a, c, d). Heterozygous *PolgA^{mut}* mice ($+/PolgA^{mut}$) were intercrossed to generate mtDNA-mutator mice ($PolgA^{mut}/PolgA^{mut}$). This cross resulted in normal litter sizes (mean litter size 8.9 pups) and mendelian distributions of genotypes ($n = 500$ genotyped animals; wild type 25.8%, $+/PolgA^{mut}$ 50.1% and $PolgA^{mut}/PolgA^{mut}$ 24.1%) showing that homozygosity for *PolgA^{mut}* allele does not result in embryonic or early postnatal lethality. We followed the survival of wild-type ($n = 50$) and mtDNA-mutator ($n = 38$) mice (Fig. 2e). A total of 18 mtDNA-mutator mice died spontaneously, whereas the remaining 20 mice were killed in accordance with the ethical permit requirements because of moribund appearance. Standard Southern blot protocols were used for genotyping.

Analyses of DNA polymerase and exonuclease activities

A recombinant mtDNA polymerase holoenzyme was obtained by co-expression of human POLGA and POLGB subunits in the baculovirus system and biochemical purification. The DNA polymerase activities of recombinant proteins and mitochondrial extracts were determined by measuring incorporation of $[\alpha\text{-}^{32}P]dTTP$ into the artificial $(rA).p(dT)_{12-18}$ template. The exonuclease activities of recombinant proteins were determined by adding a substrate obtained by annealing a $5'$ ^{32}P-labelled 21-base oligonucleotide ($5'$-TGCATGCCTGCAGGTCGACTG-$3'$) to M13mp18 single-stranded DNA (Biolab). This substrate consists of a 20-base-pair double-stranded region with a one-nucleotide $3'$ mismatch. The exonuclease reactions were analysed by electrophoresis in 3 M urea/25% polyacrylamide gels.

Quantification of lean body mass, body fat, BMD and BMC

Mice were killed by CO_2 inhalation and densitometry was performed by using a PIXImus imager (GE Lunar). A total of three wild-type and three mtDNA-mutator mice were analysed at the age of 20 weeks, and five wild-type and five mtDNA-mutator mice were analysed at the age of 40 weeks. Body fat (percentage), lean body mass, BMD ($g\,cm^{-2}$) and BMC (g) were determined in the whole mouse. BMD and BMC were also determined in the dissected femur bone. Field calibration and calibration versus the quality control phantom were performed each day before mouse or femur imaging.

Analysis of mtDNA mutations

Total DNA was extracted from the brains of 2-month-old wild-type, heterozygous and mtDNA-mutator mice. Enriched mtDNA was extracted from the isolated mitochondria (prepared by differential centrifugation) of different tissues of 6-month-old mice. The somatic mtDNA mutation load was determined by PCR, cloning, and sequencing, as described earlier[28], using primers that specifically amplified the cytochrome *b* gene (nucleotide pair 14,073–14,906) and non-coding control region (15,357–138) of mouse mtDNA[29] (GenBank NC_005089) together with flanking sequences.

Histology and biochemical analyses

Different tissues were fixed in buffered formalin, embedded in paraffin, sectioned and stained with haematoxylin and eosin. Enzyme histochemical and ultrastructural analyses of myocardium were performed as described[25,26]. The measurement of respiratory chain enzyme complex activities, citrate synthase activity and MAPR was performed as previously described[25,26,30].

1. Corral-Debrinski, M. *et al.* Mitochondrial DNA deletions in human brain: regional variability and increase with advanced age. *Nature Genet.* **2,** 324–329 (1992).
2. Schwarze, S. R. *et al.* High levels of mitochondrial DNA deletions in skeletal muscle of old rhesus monkeys. *Mech. Ageing Dev.* **83,** 91–101 (1995).
3. Khaidakov, M., Heflich, R. H., Manjanatha, M. G., Myers, M. B. & Aidoo, A. Accumulation of point mutations in mitochondrial DNA of aging mice. *Mutat. Res.* **526,** 1–7 (2003).
4. Mueller-Hocker, J. Cytochrome-c-oxidase deficient cardiomyocytes in the human heart—An age-related phenomenon. *Am. J. Pathol.* **134,** 1167–1173 (1989).
5. Fayet, G. *et al.* Ageing muscle: clonal expansions of mitochondrial DNA point mutations and deletions cause focal impairment of mitochondrial function. *Neuromuscul. Disord.* **12,** 484–493 (2002).
6. Cottrell, D. A. *et al.* Cytochrome c oxidase deficient cells accumulate in the hippocampus and choroid plexus with age. *Neurobiol. Aging* **22,** 265–272 (2001).
7. Cottrell, D. A. & Turnbull, D. M. Mitochondria and ageing. *Curr. Opin. Clin. Nutr. Metab. Care* **3,** 473–478 (2000).
8. Wallace, D. C. A mitochondrial paradigm for degenerative diseases and ageing. *Novartis Found. Symp.* **235,** 247–263 (2001).
9. Carrodeguas, J. A., Kobayashi, R., Lim, S. E., Copeland, W. C. & Bogenhagen, D. F. The accessory subunit of *Xenopus laevis* mitochondrial DNA polymerase γ increases processivity of the catalytic subunit of human DNA polymerase γ and is related to class II aminoacyl-tRNA synthetases. *Mol. Cell. Biol.* **19,** 4039–4046 (1999).
10. Foury, F. & Vanderstraeten, S. Yeast mitochondrial DNA mutators with deficient proofreading exonucleolytic activity. *EMBO J.* **11,** 2717–2726 (1992).
11. Vanderstraeten, S., Van den Brule, S., Hu, J. & Foury, F. The role of $3'$-$5'$ exonucleolytic proofreading and mismatch repair in yeast mitochondrial DNA error avoidance. *J. Biol. Chem.* **273,** 23690–23697 (1998).
12. Rodriguez, C. I. *et al.* High-efficiency deleter mice show that FLPe is an alternative to Cre–*loxP*. *Nature Genet.* **25,** 139–140 (2000).
13. Meyers, E. N., Lewandoski, M. & Martin, G. R. An Fgf8 mutant allelic series generated by Cre- and Flp-mediated recombination. *Nature Genet.* **18,** 136–141 (1998).
14. Kalu, D. N. *Handbook of Physiology* section 11 *Aging* (Oxford Univ. Press, New York, 1995).
15. Arking, R. *Biology of Aging* (Sinauer, Sunderland, Massachusetts, 1998).
16. Haines, D. C., Chattopadhyay, S. & Ward, J. M. Pathology of aging B6;129 mice. *Toxicol. Pathol.* **29,** 653–661 (2001).
17. Weiss, A., Arbell, I., Steinhagen-Thiessen, E. & Silbermann, M. Structural changes in aging bone: osteopenia in the proximal femurs of female mice. *Bone* **12,** 165–172 (1991).
18. Balducci, L. Epidemiology of anemia in the elderly: information on diagnostic evaluation. *J. Am. Geriatr. Soc.* **51,** S2–S9 (2003).
19. Braunwald, E. (ed.) *Heart Disease. A Textbook of Cardiovascular Medicine* (W.B. Saunders Co., Philadelphia, 1997).
20. Pal, L. & Santoro, N. Age-related decline in fertility. *Endocrinol. Metab. Clin. North Am.* **32,** 669–688 (2003).
21. Tanemura, K., Kurohmaru, M., Kuramoto, K. & Hayashi, Y. Age-related morphological changes in the testis of the BDF1 mouse. *J. Vet. Med. Sci.* **55,** 703–710 (1993).
22. Larsson, N. G. *et al.* Mitochondrial transcription factor A is necessary for mtDNA maintenance and embryogenesis in mice. *Nature Genet.* **18,** 231–236 (1998).
23. Silva, J. P. *et al.* Impaired insulin secretion and β-cell loss in tissue-specific knockout mice with mitochondrial diabetes. *Nature Genet.* **26,** 336–340 (2000).
24. Sorensen, L. *et al.* Late-onset corticohippocampal neurodepletion attributable to catastrophic failure of oxidative phosphorylation in MILON mice. *J. Neurosci.* **21,** 8082–8090 (2001).
25. Hansson, A. *et al.* A switch in metabolism precedes increased mitochondrial biogenesis in respiratory chain-deficient mouse hearts. *Proc. Natl Acad. Sci. USA* **101,** 3136–3141 (2004).
26. Wredenberg, A. *et al.* Increased mitochondrial mass in mitochondrial myopathy mice. *Proc. Natl Acad. Sci. USA* **99,** 15066–15071 (2002).
27. Wang, J., Silva, J., Gustafsson, C. M., Rustin, P. & Larsson, N. G. Increased *in vivo* apoptosis in cells lacking mitochondrial DNA gene expression. *Proc. Natl Acad. Sci. USA* **98,** 4038–4043 (2001).
28. Spelbrink, J. N. *et al. In vivo* functional analysis of the human mitochondrial DNA polymerase POLG expressed in cultured human cells. *J. Biol. Chem.* **275,** 24818–24828 (2000).
29. Bibb, M. J., VanEtten, R. A., Wright, C. T., Walberg, M. W. & Clayton, D. A. Sequence and organization of mouse mitochondrial DNA. *Cell* **26,** 167–180 (1981).
30. Wibom, R., Hagenfeldt, L. & von Dobeln, U. Measurement of ATP production and respiratory chain enzyme activities in mitochondria isolated from small muscle biopsy samples. *Anal. Biochem.* **311,** 139–151 (2002).

....

An autonomous molecular computer for logical control of gene expression

Yaakov Benenson[1,2], Binyamin Gil[2], Uri Ben-Dor[1], Rivka Adar[2] & Ehud Shapiro[1,2]

[1]*Department of Computer Science and Applied Mathematics and* [2]*Department of Biological Chemistry, Weizmann Institute of Science, Rehovot 76100, Israel*

....

Early biomolecular computer research focused on laboratory-scale, human-operated computers for complex computational problems[1–7]. Recently, simple molecular-scale autonomous programmable computers were demonstrated[8–15] allowing both input and output information to be in molecular form. Such computers, using biological molecules as input data and biologically active molecules as outputs, could produce a system for 'logical' control of biological processes. Here we describe an autonomous biomolecular computer that, at least *in vitro*, logically analyses the